Additive Manufacturing 32 (2020) 100993

Contents lists available at ScienceDirect

Additive Manufacturing

journal homepage: www.elsevier.com/locate/addma

Full Length Article

Melt pool size control through multiple closed-loop modalities in laser-wire directed energy deposition of Ti-6Al-4V*

B.T. Gibson[a,*], Y.K. Bandari[b], B.S. Richardson[a], W.C. Henry[c], E.J. Vetland[c], T.W. Sundermann[d], L.J. Love[a]

[a] Manufacturing Demonstration Facility, Energy and Transportation Science Division, Oak Ridge National Laboratory, Knoxville, TN, 37932, USA
[b] EWI - Buffalo Manufacturing Works, Buffalo, NY, 14203, USA
[c] GKN Aerospace, Hazelwood, MO, 63042, USA
[d] University of Nebraska, Lincoln, NE, 68588, USA

ARTICLE INFO

Keywords:
Additive manufacturing
3D printing
Directed energy deposition
Lasers
Melt pool
Monitoring
Closed-loop
Control
Metal
Ti-6Al-4V

ABSTRACT

Sensing and closed-loop control are critical attributes of a robust 3D printing process, such as Directed Energy Deposition (DED), in which it is necessary to manage geometry, material properties, and residual stress and distortion. The present research demonstrates multiple modes of closed-loop melt pool size control in laser-wire based DED, a form of large-scale metal additive manufacturing. First, real-time closed-loop melt pool size control through laser power modulation was demonstrated for intralayer control of bead geometry. Aspects such as controller tuning, response time, interaction with primary process variables, and disturbance rejection are presented. Next, an interlayer trend in laser power during the printing of layered components was documented, which inspired the development of novel modes of control. A controller that modulates print speed and deposition rate on a per-layer basis was developed and demonstrated, enabling the control of either average melt pool size alone or average laser power in coordination with real-time melt pool size control. This work demonstrates that accumulated heat in components under construction can be exploited to maintain process stability as print speed and deposition rate are automatically increased under closed-loop control. This has major implications for overall production efficiency. Control modes are characterized in terms of their effect on local bead geometry, global part geometry, and interlayer effect on energy density, among other factors.

1. Introduction

Large-scale metal additive manufacturing (AM), also known as metal Big Area Additive Manufacturing (m-BAAM), has captured the attention of manufacturers who are seeking alternative production processes for large metallic components that are currently associated with high costs and long lead times. Industries potentially impacted by this disruptive technology include the tool-and-die and the aerospace industries, among others. In the aerospace industry, the driving forces for change are the high costs and lead times of pre-forms, or forgings, for Ti-6Al-4 V structures, as well as high buy-to-fly ratios, a metric that quantifies the significant scrap that is produced from machining components made from large billets or forgings. AM affords the opportunity to fabricate pre-forms in rapid design-and-production cycles and to produce near net-shape components that significantly reduce buy-to-fly ratios. Directed Energy Deposition (DED) is a family of AM technologies that is the focus of attention for printing large freeform structures with either metallic wire or powder as the feedstock and a laser, electric arc, or electron beam as the heat source.

The grand challenge associated with these processes, however, is simultaneous control of geometry, material properties, and residual stress and distortion. Researchers are deploying a wide array of

Abbreviations: AM, additive manufacturing; DED, Directed Energy Deposition; ED, energy density; IR, infrared radiation; LP, laser power; m-BAAM, metal Big Area Additive Manufacturing; MPS, melt pool size; NIR, near infrared radiation; PS, print speed; SA, spot area; t, time

* This manuscript has been authored by UT-Battelle, LLC under Contract No. DE-AC05-00OR22725 with the U.S. Department of Energy. The United States Government retains and the publisher, by accepting the article for publication, acknowledges that the United States Government retains a non-exclusive, paid-up, irrevocable, worldwide license to publish or reproduce the published form of this manuscript, or allow others to do so, for United States Government purposes. The Department of Energy will provide public access to these results of federally sponsored research in accordance with the DOE Public Access Plan (http://energy.gov/downloads/doe-public-access-plan).

* Corresponding author.
E-mail address: gibsonbt@ornl.gov (B.T. Gibson).

https://doi.org/10.1016/j.addma.2019.100993
Received 30 September 2019; Received in revised form 25 November 2019; Accepted 7 December 2019
Available online 23 December 2019
2214-8604/ © 2019 Elsevier B.V. All rights reserved.

techniques to address this challenge. Pre-print modeling and simulation, as well as characterization of post-print materials, are commonly used to correlate the selection of process variables (e.g. laser power, deposition rate, and print speed) with the resulting material properties and residual stress and distortion. Artificial intelligence and machine learning techniques are also being utilized to establish these correlations and, further, to correlate in-process signals with the resulting material properties and location-specific defects.

A key enabler of these techniques is a robust ability to collect useful signals during the printing process. Accordingly, sensing deposition geometry, temperatures, and melt pool morphology has been the focus of significant research. Additionally, useful signals collected in real-time present the opportunity for closed-loop control of geometry or thermal properties. Closed-loop control in AM is highly desirable in that printing conditions are managed in real-time, and the front-end workload on the user is reduced such that less predictive modeling and simulation is required. Closed-loop control also means that certain build constraints, such as consistent interpass times, are relaxed, and unforeseen build characteristics or disruptions can be handled automatically. In DED, closed-loop control of melt pool size (MPS) is particularly desirable because MPS is a highly useful signal in which the thermal properties of the build are reflected and there is a potential for fine control of bead geometry.

The available literature on MPS control in DED is heavily weighted toward powder-based DED, which has demonstrated closed-loop control and has documented several efforts to manage MPS through predictive modeling and simulation. As an alternative to melt pool monitoring and closed-loop control, Aggarangsi et al. developed and modeled laser power reduction schedules as a method of MPS management while depositing in certain transient situations in laser-powder based DED [1]. Vasinonta et al. took a process-mapping based approach to controlling MPS in laser-powder based DED and also explored the impact of build aspect ratio (thin-walled versus bulky parts) in a process mapping approach for MPS control [2,3].

With regard to closed-loop control, Beuth and Klingbeil suggested a fundamental understanding of the role of process variables in laser-powder based DED was a critical pathway [4]. Accordingly, Birnbaum et al. examined the transient MPS response to a laser power step change in powder-based DED and scaled predictions of melt pool geometry and wall thickness from a 500 W maximum laser power process to a 2700 W maximum laser power process [5]. Aggarangsi et al. predicted melt pool transients in the case of a laser power step change in laser-powder based DED and compared results against experimental measurements obtained with a thermal imaging system [6]. The difficultly in experimentally measuring response times due to noise and other factors was discussed.

Obviously, robust sensing capabilities are key to implementing successful closed-loop control, and such issues must be addressed. Meriaudeau et al. developed a thermal imaging system based on a CCD camera that would monitor the melt pool in laser cladding, a form of powder-based DED [7]. While the system was utilized for process monitoring and optimization, the authors note that because signals were available in real-time they could also be utilized for closed-loop process control. Hu et al. developed a closed-loop control system for laser cladding in which laser power was manipulated to control molten pool area [8]. The system relied upon thermal imaging with a co-axially mounted, CCD-based camera. The study showed that closed-loop control yielded improved, consistent geometry in thin-walled structures when compared to open-loop control. In terms of camera calibration and temperature measurement accuracy, the authors note that, for the purposes of closed-loop control, some leeway is allowed with respect to accuracy of absolute temperature measurements. That is, relative measurements that define a metric, such as MPS or an isotherm of MPS, are adequate as long as they consistently track with the thermal characteristics of the build.

Hofmeister et al. demonstrated closed-loop control of melt pool isotherm area in laser-powder based DED [9]. First, the authors used a high-speed digital camera mounted in-axis to image the molten pool and enable visible light radiation pyrometry. Molten pool width, length, and isotherm area were found to have smooth, consistent relationships with absorbed energy; these relationships suggested closed-loop control efforts would be successful. After closed-loop control was successfully demonstrated, the authors also documented improved dimensional accuracy of the printed components.

Hu and Kovacevic experimentally validated a finite element model of cooling rate in laser-powder based DED by printing single-bead walls with and without closed-loop melt pool width control [10]. Laser power was modulated to achieve the desired melt pool width. The melt pool was imaged using a dual camera system that included a CCD-based camera with near infrared (NIR) filtering and a high-speed camera with synchronized shuttering and a secondary illuminating laser to confirm the location of the molten pool edge. Control success was demonstrated from a comparison of the final printed wall geometries.

Examining the literature associated with other DED processes, Zalameda et al. presented a closed-loop control system for maintaining molten pool area through adjustment of beam power in the Electron Beam Freeform Fabrication (EBF^3) process, which is a form of wire-fed DED [11]. Off-axis imaging with an NIR camera was utilized to measure the temperatures of the molten pool and the trailing solidification zone. Certain measured intensities were selected to delineate regions of interest and define the molten pool and tail areas. During bead depositions, the authors observed that the tail area, but not the molten pool area, was sensitive to increasing substrate temperatures throughout the deposition. Nevertheless, the authors selected molten pool area as a controlled variable for which beam power would be automatically manipulated. Single bead walls were printed to compare no control, 'manual' control, and closed-loop control. The most consistent cross-sectional area was achieved with 'manual' control. The authors noted that wire height was an additional variable for which automatic adjustments would be desired to improve closed-loop control performance. The authors also explored the possibility of using the NIR camera to perform thermal non-destructive evaluation (NDE) of deposits.

In terms of laser-wire based DED processes, Heralic et al. have been significant contributors in robotic control system development; they have demonstrated closed-loop control systems that manipulate laser power and wire feed rate in order to control bead geometry [12]. However, the overall lack of depth in the literature on thermal control of laser-wire based DED processes served as a motivating factor for the present research. In particular, a comprehensive examination of MPS control, its interactions with primary process variables, and its impact on local bead geometry and global part geometry were of interest. Additionally, an investigation into the effects of MPS control on laser power behavior and trends in the energy density within printed parts was carried out, with a vision toward exploiting these trends for a novel mode of thermal control. In all, three modes of thermal control, along with a comparison of the relative merits of each, are presented here. Because this research was conducted through a public-private partnership, some details are considered protected intellectual property and have therefore not been included in the article.

2. Methods

Depositions in this study were carried out in a custom, large-scale laser hot-wire DED workcell that contained a 6-axis industrial robot, wirefeeder, and hot wire system. The workcell was supplied by two fiber-delivered diode lasers with a combined laser power capacity of 20 kW. The hot wire system supplied relatively low-power auxiliary resistance heating of the wire prior to it entering the melt pool. Parts were printed in an Argon environment, maintained by a tent-like enclosure that surrounded the build plate and was purged prior to printing. Oxygen levels were maintained below 600 ppm throughout

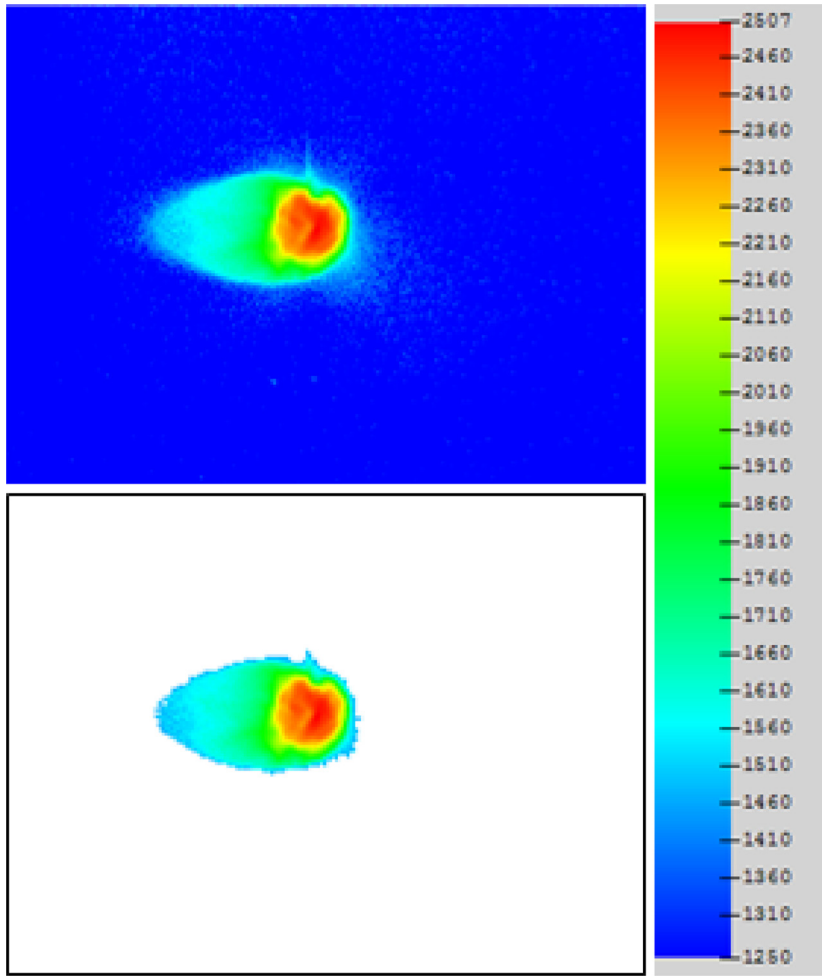

Fig. 1. Examples of As-Collected (top) and Thresholded (bottom) Melt Pool Images; Scale Units are Degrees Celsius.

the deposition process by a steady flow of Argon. All work was carried out with a 1.6 mm (0.063 inch) diameter Ti-6Al-4 V wire as the feedstock, and depositions were made on build plates of the same alloy in 6.35 mm (0.25 inch) thickness. While Ti-6Al-4 V was the focus of this work, it is believed that the methods and results presented are applicable to additional alloy systems, provided actions are taken to ensure material-specific factors are accounted for in the measurement of melt pool size.

The laser optics were instrumented with an in-axis thermal camera for imaging the melt pool in real-time. The camera receives emissions from the melt pool through the laser optics via a dichroic mirror. Narrow-band sensing in the IR range, below the range of laser wavelengths, was accomplished with filtering, and the resulting thermal field was software-thresholded to define a melt pool size and shape. Examples of as-collected and thresholded melt pool thermal field images from the system during a side-feed deposition are displayed in Fig. 1. Additional details regarding the development of this system, specifically challenges that are unique to the laser hot-wire DED process, including methods for filtering, noise reduction, and selection of exposure rate for generating high quality images of the melt pool, as well as correlation of pixels with real MPS, are available in prior work [13]. In prior work on the development of melt pool imaging and definition, rather than focusing on identification and thorough characterization of the transition zone between the molten pool and solidified metal, emphasis was placed on identifying a low-noise melt pool definition. Additionally, the imaging technique was developed to ensure that the area of the defined melt pool, determined via a summation of pixels, would track consistently with thermal conditions of the build.

Additional print head instrumentation included an in-axis visible camera for monitoring the wire input location and process stability, and a laser line scanner for sensing build height relative to the nominal ideal layer height (this is discussed further in a following section).

The thermal imaging system provided real-time measurements of the MPS to a closed-loop controller that operated at 200 Hz, which enabled laser power to be modulated in real-time to control MPS at a desired value; this mode of operation is known as Mode 1. Measurements of MPS and laser power were also provided to a layer monitor in which layer statistics, such as average size or power, were computed. In another tested mode of operation (Mode 2), average MPS was controlled on a per-layer basis by manipulating print speed and nominal deposition rate, which were maintained at a consistent ratio as they were modulated. A final mode (Mode 3) combined attributes of the first two modes, in that laser power was modulated to control MPS in real-time, and print speed and nominal deposition rate were modulated on a per-layer basis to control average laser power. These control modes are summarized in Table 1. While other modes of control are certainly

Table 1
Control Modes.

Control Mode	Controlled Variable	Manipulated Variable	Cycle
0	None	N/A	N/A
1	Melt Pool Size	Laser Power	Real-time
2	Average Melt Pool Size	Print Speed & Dep. Rate	Layerwise
3	Melt Pool Size	Laser Power	Real-time
	Average Laser Power	Print Speed & Dep. Rate	Layerwise

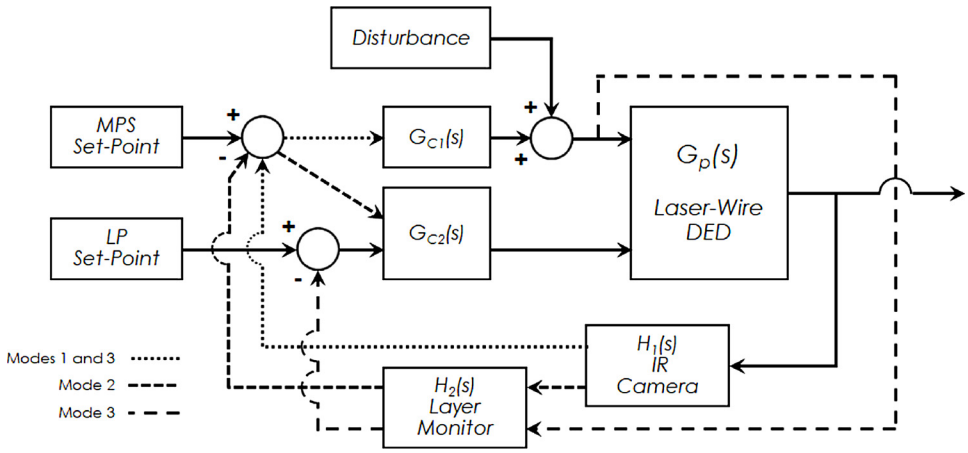

Fig. 2. Controller Architecture.

possible, temperature control being one alternative that has been proposed in the literature, the three modes of control selected for testing were believed to have the most promise with respect to geometry control and process efficiency.

The control architecture for Modes 1–3 is displayed in Fig. 2. Mode-dependent paths are shown with dotted lines. The architecture contained two controllers that could operate independently or concurrently, depending on the control mode. The specific control laws varied with mode of operation but are considered protected intellectual property, and therefore, further details have not been included in this article. The general philosophy by which set-points were determined was to consistently keep layer 1 properties. For example, in Mode 1, the set-point was typically determined by running test deposits with only melt pool monitoring (i.e., without active control) to measure average MPS, which then became the controller set-point for subsequent deposits. The system was also designed to forgo selection of an explicit set-point for average MPS in Mode 2 and average laser power in mode 3 and instead regulate based on layer 1 properties, whatever they were determined to be after layer 1 was printed.

The nominal deposition parameters used for the majority of the tests presented here are shown in Table 2; deviations from these parameters, and additional noteworthy parameters, are discussed on a case-by-case basis. Beads and walls were deposited with either the front or side feed wire orientation, with wire input angles in the range of 39° to 54° and laser lead angles in the range of -6° to 9°.

Laser power delivered to the substrate was determined through a calibration process that used a power puck measurement device. The deposition rate of 2.4 kg/hr is a function of wire speed, wire diameter, and wire density, which was assumed to be 4.43 g/cm^3. The corresponding nominal wire speed was 75 mm/s.

Initial explorations into MPS control were carried out as an exercise in Mode 1 control of bead-on-plate depositions. This involved step changes in the MPS set-point while maintaining constant print speeds and deposition rates. Beads were initiated with a constant laser power. After the MPS reached a desired threshold (2000 pixels for this particular test), the controller turned on. The melt pool set-point was then commanded to step up from 2600 pixels to 3400 pixels and back down to 2600 pixels during a single bead, a step magnitude of 31 %. This test

Table 2
Primary Process Parameters.

Parameter	Value	Units
Delivered Laser Power	8.71	kW
Deposition Rate	2.4	kg/hr
Print Speed	8	mm/s
Hot Wire Power	370	W

also provided the opportunity for tuning of the $G_{C1}(s)$ controller, which was carried out with the goal of achieving a fast response time while minimizing noise. Gains were tuned in a sequential, iterative method while depositing a series of beads with step changes. Further details regarding controller gains, including the values determined to yield the desired response, are considered protected intellectual property; however, a comparison of system responses before and after tuning is presented.

Deposits were also examined to document the changes in bead geometry that manifested from MPS set-point changes. Typically, controllers are tuned with the primary objective of performing either set-point tracking or disturbance rejection, and while set-point changes were used as a tuning exercise, the disturbance rejection capabilities of the controller are important for the laser-wire DED processes. Therefore, two additional developmental tests were carried out under Mode 1 control with the goal of examining disturbance rejection. First, changes in print speed were commanded within a single bead, from an initial speed of 8 mm/s to 4 mm/s and then 12 mm/s, while maintaining a constant deposition rate. Laser power was modulated to maintain the MPS at a set-point of 3600 pixels. Bead geometry was examined and compared against the same test carried out under Mode 0 with constant laser power. Secondly, tests were carried out in which beads were deposited with a constant print speed, deposition rate, and MPS set-point (2400 pixels), but laser power disturbances (offsets) were added to the control signal at the location indicated in Fig. 2. Laser power offsets of 0.5 kW and 1 kW in magnitude were tested to study how the controller managed the introduction of the disturbances.

Single bead walls were printed to test the thermal control modes, some of which (Modes 2 and 3) are inherently driven by layerwise trends, during the deposition of 3D components. Walls were 175 mm long and approximately 100 mm tall (63 layers with a 1.6 mm nominal layer height); bead width was approximately 12 mm. The wire orientation was front feed, except for a bead termination routine that was executed at the end of each layer, in which the print head reversed and deposited additional material for a prescribed distance along the toolpath. This routine combats the slumping that can occur at the end of walls, in the region of bead termination. The prescribed reversal distance, nominal deposition rate, and laser power evolved within the routine for a set number of layers, after which they were constant in the routine. The parameters utilized for the bead termination routine are shown in Table 3.

In addition to controlling geometry, the bead termination routine also created highly transient process conditions in which the behavior of the system under different control modes could be compared. Deposition rate also varied in real-time during wall printing due to a height control system. To control layer height and drive the changes in deposition rate, the height control system utilized the laser line scanner

Table 3
Bead Termination Routine Parameters.

Parameter	Value	Units
Initial Distance	10	mm
Distance Increment	1	mm
Laser Power Increment[a]	0	%
Deposition Rate Increment	−1.2	%
Maximum Layer	20	

[a] Applicable only to Modes 0 and 2, in which laser power is not manipulated in real-time.

to measure deposited geometry and compare it against the ideal geometry. Further details of this specific height control system and its behavior have been described in ref [14]. After depositions were complete, walls were scanned using a FaroArm scanner to create a virtual 3D representation of each wall and allow for comparisons between the global part geometries produced by the different control modes.

An explicit set-point for MPS (2500 pixels) was selected for Mode 1 and Mode 3 walls. The Mode 2 set-point for average MPS and Mode 3 set-point for average laser power were based on the averages during layer 1. Tuning of the $G_{C2}(s)$ controller was accomplished by iteratively adjusting the controller gain, to reduce noise and maintain performance, in between a series of wall prints. The primary metrics presented are interlayer trends in MPS, laser power, print speed, deposition rate, and the resulting energy density. These metrics allow for comparisons of the system behavior produced by the different control modes. Intralayer, or within-layer, control behavior is presented on a limited-basis as well.

Finally, a second geometry was printed to provide a largely qualitative comparison of the bead geometries produced by control Modes 0 and 1. This comparison provides additional evidence for the merits of control. The geometry was a closed-contour, elliptical tool path with a major axis 175 mm in length and a minor axis 34 mm in length, in which the bead initiation/termination point rotated among the four quadrants on a per layer basis. Wire orientation varied continuously throughout the toolpath, and no bead termination routine was required for this geometry. While this geometry is not a primary focus of this article, it provides a compelling visual comparison of parts printed with and without thermal control.

3. Results

3.1. Melt pool size control development tests

An example of step changes in MPS before controller tuning is shown in Fig. 3. The figure also indicates the point at which the laser turned on, the starting laser power, the point at which the controller turned on, and the point at which the laser turned off. The MPS command, showing the step changes, is indicated as well. The MPS was commanded up at approximately 12 s and back down at approximately 24 s. Laser power was modulated to achieve the desired melt pool sizes. Again, beads were deposited with a constant deposition rate for this test, i.e. wire feed rate did not increase with higher laser powers, but the process remained in the stable range (no droplet transfer of the wire into the melt pool was observed).

Also shown in Fig. 3 is an example of step changes in MPS after controller tuning. Without tuning, the response time for the MPS step from 2600 to 3400 pixels was approximately 0.44 s, with some overshoot present. The response time for the MPS step from 3400 pixels back down to 2600 pixels was approximately 0.6 s. While the response time was considered adequate and no major oscillations were observed in the controller response, there was an undesirable level of noise in both the MPS and laser power signals. A noticeable level of noise reduction was achieved through the controller tuning process. Examining response times for the tuned example, the time for the MPS step from 2600 to 3400 pixels was approximately 0.27 s, and the response time for the MPS step from 3400 pixels back down to 2600 pixels was approximately 0.48 s. With proper tuning, laser power modulated more effectively to decrease the response time; this is evident as large, distinct laser power fluctuations at the points of step-change. The 0.48 response time, at a print speed of 8 mm/s, would correspond to a maximum travel distance of 3.8 mm over which the bead geometry would transition. This response time was considered to be adequate and suitable for industrial implementation of this control technique. A further characterization of the melt pool response was not considered to be within the scope of this work; however, a further examination of melt pool dynamic behavior for this specific laser-wire DED process has been presented in ref [15].

The bead geometries that manifested from the step changes in MPS are shown in Fig. 4. Bead width increased and decreased noticeably with the MPS changes. Because the deposition rate and print speed were constant, a consistent bead cross-sectional area with a change in cross-section profile (wider and shorter) was expected.

The results for MPS control in the presence of print speed step changes are shown in Fig. 5. The system response is intriguing because the step changes in print speed are nearly instantaneous, while there is a more gradual, transient response in laser power that lags the print speed changes, particularly for the step from 8 mm/s to 4 mm/s. In terms of magnitude, laser power fluctuated over a range of approximately 4 kW, highlighting the significant degree to which changes in primary process parameters, e.g. print speed, can influence MPS. MPS was nicely controlled through the step changes, with the exception of the 12 mm/s print speed section, in which laser power increased to the point of saturation; this test was carried out using only a single laser, which has a maximum output of 10.7 kW. The time at which laser power reached the point of saturation is indicated in Fig. 5, and there is a corresponding slight decrease in MPS in that region. The resulting bead geometry for this test is also shown in Fig. 4, alongside a bead containing step changes in print speed but no MPS control, i.e. Mode 0 of operation with constant laser power. In Mode 0, bead width varied noticeably with print speed, while in Mode 1 bead width was largely controlled, with the exception of some transients evident at the print speed transition points and a slight steady-state width increase in the 4 mm/s print speed section. Because deposition rate was constant, while print speed varied, changes in bead cross-sectional area were expected, regardless of control mode, due to varying amounts of material deposited per unit length. What is interesting, however, is how control mode influenced bead profile, with Mode 1 maintaining nominal bead width relatively well, and as such, the resulting bead increased in height instead.

The results of the additional disturbance rejection test are displayed in Fig. 6. The system response is evident in terms of both the dynamic and steady-state characteristics. To examine the steady-state laser power response, the mean laser power was computed for regions before and after the introduction of the disturbance, values of which are indicated in the figure. In both test cases, the laser power was reduced by the approximate magnitude of the disturbance, as would be expected. However, the dynamic response was different for the 0.5 kW and the 1 kW test cases. An oscillation in laser power, and a corresponding oscillation in MPS, was observed for the 0.5 kW test case. In the 1 kW test case, a near monotonic decrease in laser power and very little, if any, fluctuation in MPS were observed. It is suspected that the timing of the disturbance introductions, relative to the rising or falling noise in the laser power and MPS signals, was a major contributor to the very different dynamic response behaviors.

3.2. Control mode comparison in the printing of layered components

The dynamic behavior of the system was certainly of interest during the printing of the single bead walls, particularly with respect to

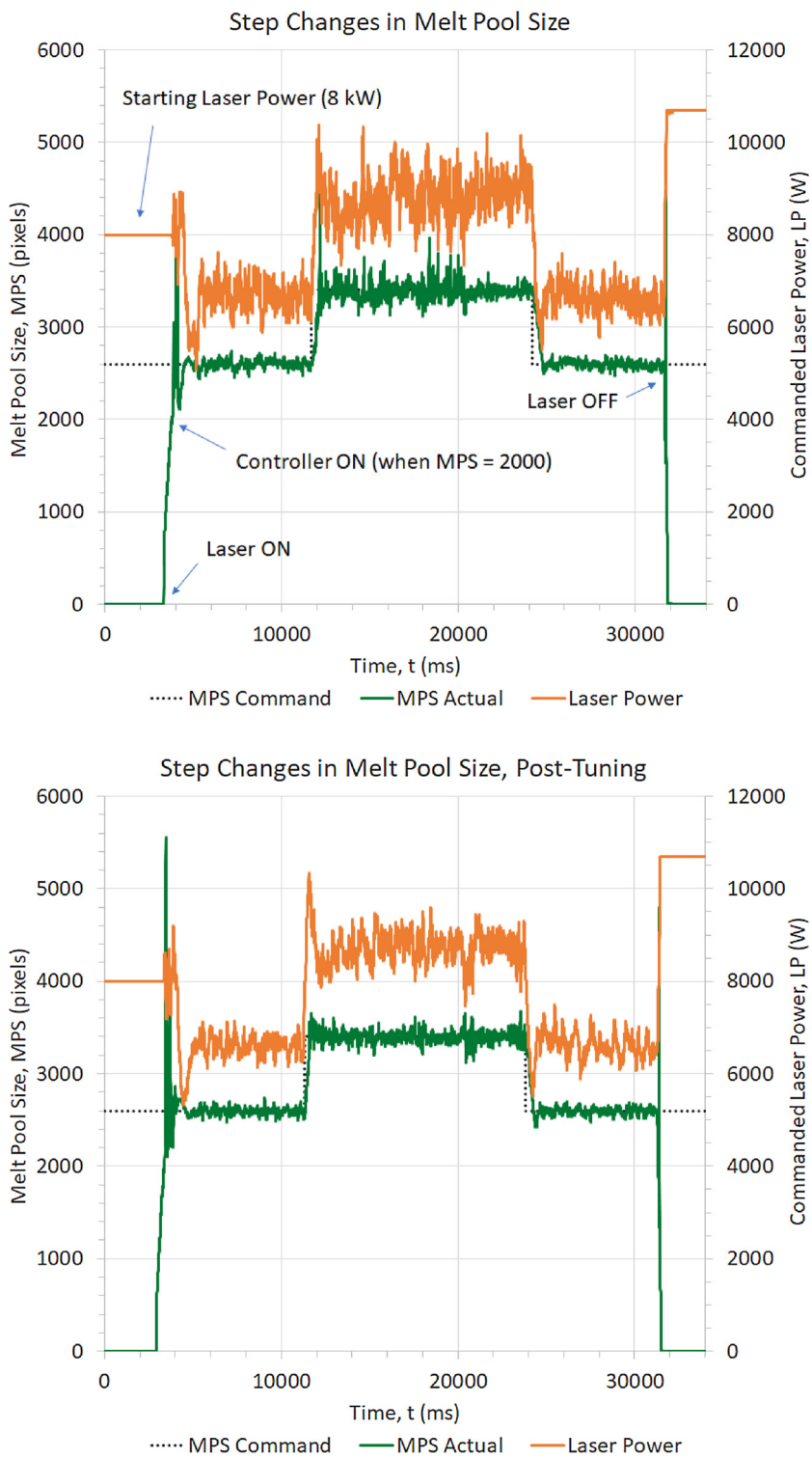

Fig. 3. Step Changes in Melt Pool Size, Pre-Tuning (Top) and Post-Tuning (Bottom).

intralayer control in the region of the bead termination routine. A photograph of one of the single bead walls printed with real-time MPS control (Mode 3) is shown in Fig. 7, and Fig. 8 shows an example of laser power during intralayer MPS control of layer 1. To achieve the desired MPS, laser power was modulated at bead initiation and the desired size was maintained throughout the length of the toolpath. Upon entering the region of bead termination, at which the print head reverses, laser power significantly decreased to approximately 4 kW. This maintained the MPS, with slight error, under highly transient conditions. Without control, bead termination would normally result in large increases in MPS and a corresponding bulging of the wall width. This is documented both in prior work [13] and here, in a following section, with photographic evidence and wall profiles from post-build scans of builds done with operation Modes 0 and 2, which do not feature real-time MPS control. The within-layer behavior of the system for both Modes 1 and 3 denoted a fine intralayer control of MPS. An additional example of this control is shown in Fig. 9, which contains photographs of the contour geometry printed with Modes 0 and 1.

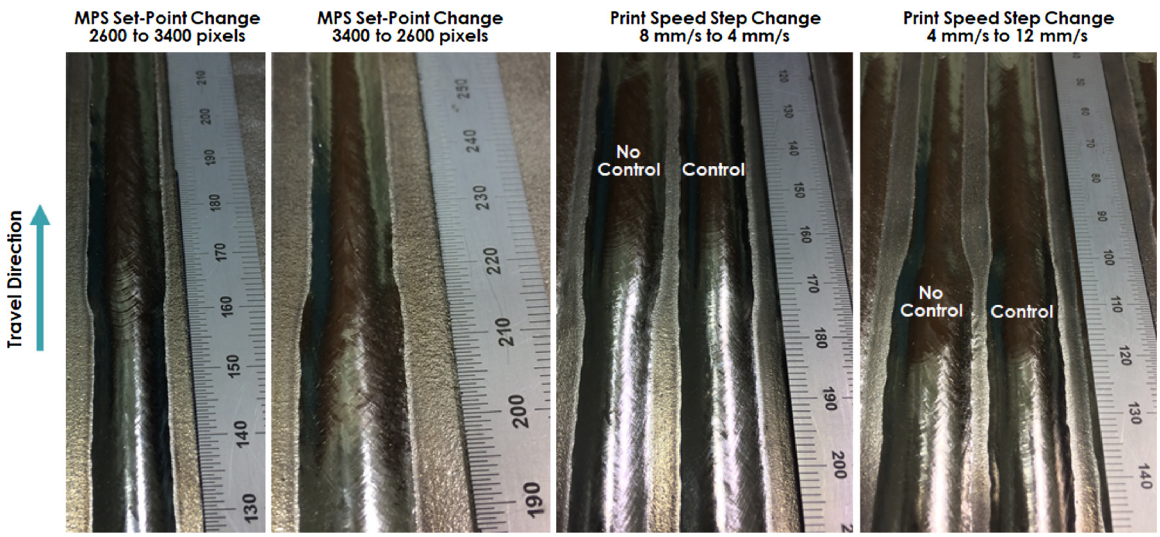

Fig. 4. Bead Geometry Resulting from Step Changes in MPS Set-Point and Print Speed.

There is a stark contrast in the bead geometry in the sharp turns at the end of the contours.

Fig. 10 displays the interlayer laser power and MPS metrics of the Mode 1 wall, compared against those of the Mode 0 wall. Note that the Mode 0 wall was printed with constant laser power, and the average MPS increased throughout the printing of the wall following a slight decrease over the initial layers. This decrease is normal and known to be driven by a geometric effect that overrides the thermal effect in the initial layers of a wall, which manifests as a slight narrowing of wall width. This effect has been documented in prior work [13] and is discussed further here with respect to 3D scans of wall geometry. In addition to the increased average MPS observed with Mode 0, the MPS range also significantly increased, with maximums extending much higher, largely driven by the higher melt pool sizes in the bead termination routine.

In contrast, the mode 1 wall exhibited melt pool sizes that were controlled with relatively low error, −4.5 % to +4.7 %, as evidenced by the narrow MPS ranges, even within the highly transient bead termination routine. There was a coarse interlayer effect associated with Mode 1 of operation that was driven by the thermal properties of the build. As heat accumulates in a part, layer-by-layer, less laser power is required to achieve the desired MPS. This is evidenced by the interlayer trend, which shows an initial increase of average laser power to combat the geometric effect in the initial layers, followed by a decrease as heat accumulated in the build. As the build progressed, average laser power decreased by approximately 2 kW, reaching a minimum average on layer 53. Laser power range increased as well, as greater modulations were required to achieve intralayer control.

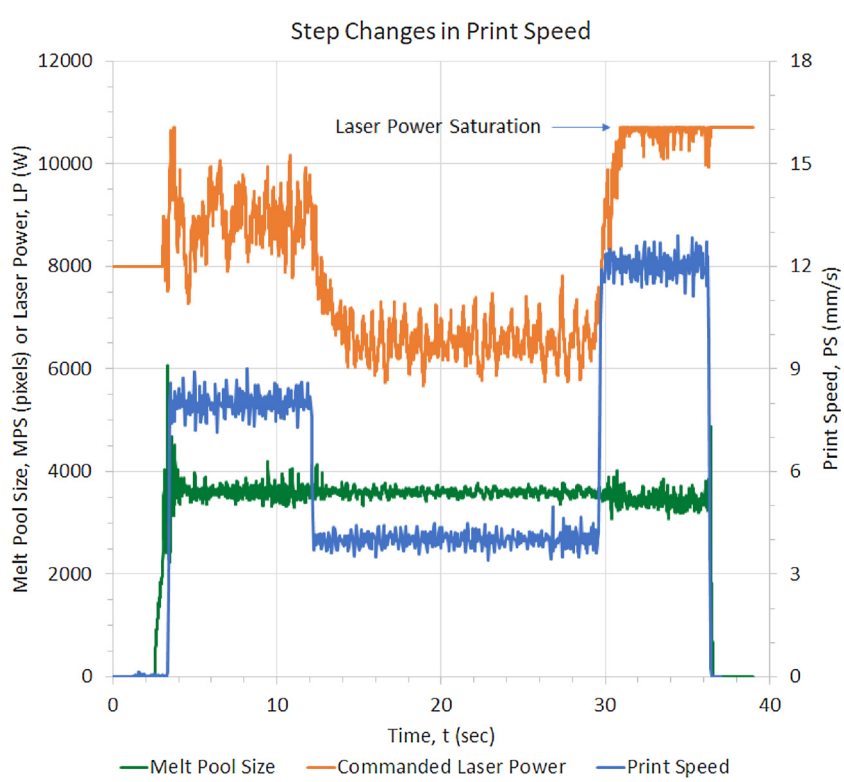

Fig. 5. System Response to Step Changes in Print Speed.

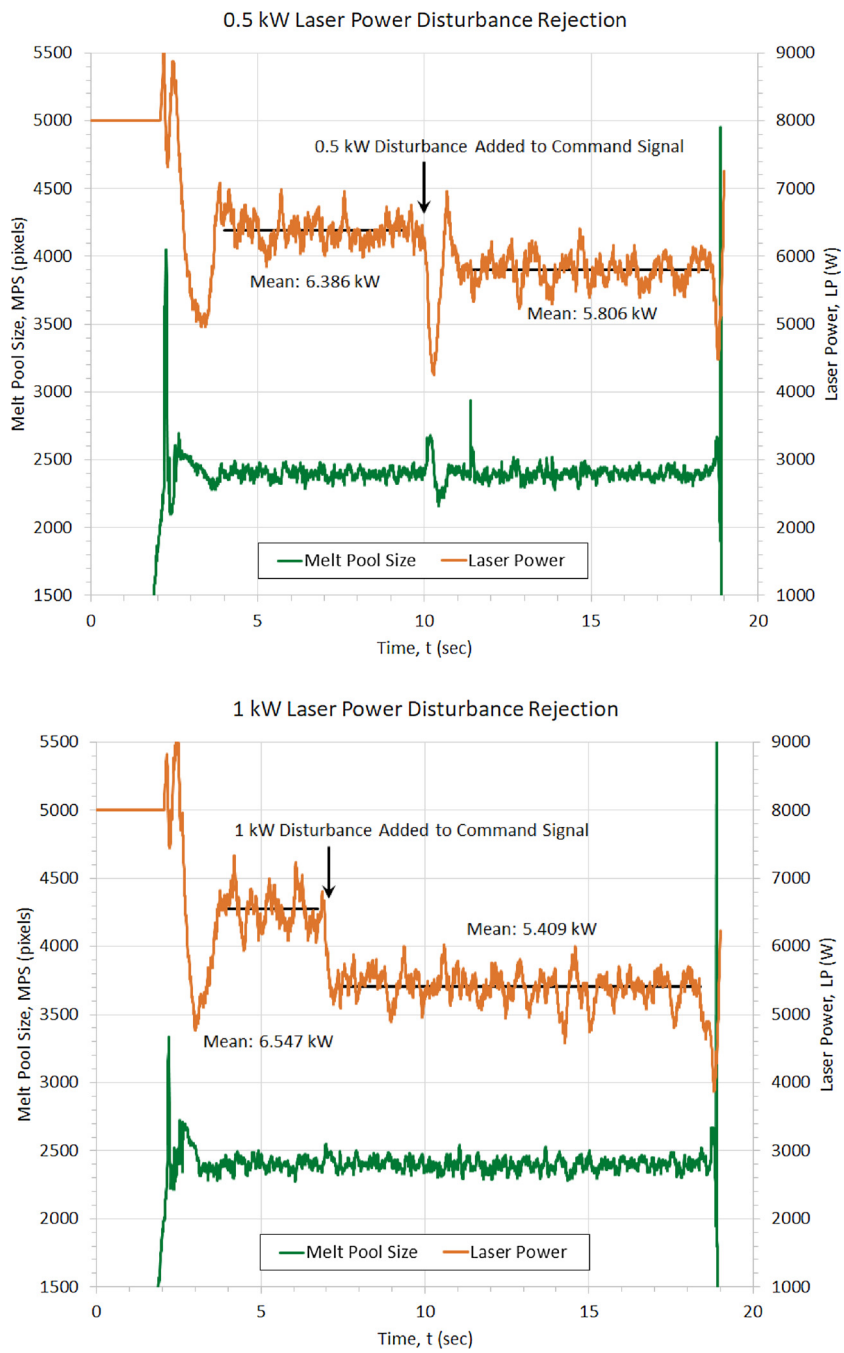

Fig. 6. Results of Laser Power Disturbance Rejection Tests.

Mode 2, like Mode 0, had no intralayer, real-time control of MPS. Rather, average MPS was controlled on a per-layer basis. In comparison to Mode 0, the ranges of MPS were decreased. The region of bead termination from the Mode 2 wall is shown in Fig. 9, in which a large bulb of material manifested from the lack of intralayer MPS control; contrast this with the region of bead termination from Mode 3, shown in Fig. 7.

Fig. 11 displays the interlayer metrics of MPS, print speed, and deposition rate for the Mode 0 and 2 walls. Because print speed and deposition rate were maintained at a consistent ratio, their modulation is plotted as a single, normalized curve. The set-point for Mode 2 was 2471.3 pixels, based on the average size of layer 1. For Mode 2, print speed increased from 8 mm/s to a peak of 11.03 mm/s and deposition rate proportionally increased from 2.4 kg/hr to a peak of 3.32 kg/hr, a 38 % increase. This led to a reduction in total print time, from 74.7 min in Mode 0 and 72.5 in Mode 1–66.4 minutes in Mode 2 (variance in interlayer data processing times can lead to slight variations in total print time, even when two cases should ideally have identical print times, as with Modes 0 and 1). Note that print speed saturators were set such that the controller could not decrease print speed below nominal, which would contrast with what is desired from a process efficiency standpoint. Because of this, there was a decrease in average MPS over the initial layers printed with Mode 2, just as with Mode 0. Remember that the initial layers are the region in which the controller would have decreased print speed to combat the previously discussed geometric effect.

Fig. 12 displays the metrics of laser power, print speed, and deposition rate for the Mode 3 wall, in comparison to those of Mode 1. Interlayer MPS for Mode 3 is not displayed, because it closely matched that of Mode 1, shown in Fig. 10. In Mode 3, print speed and deposition rate were proportionally modulated to control average laser power on a

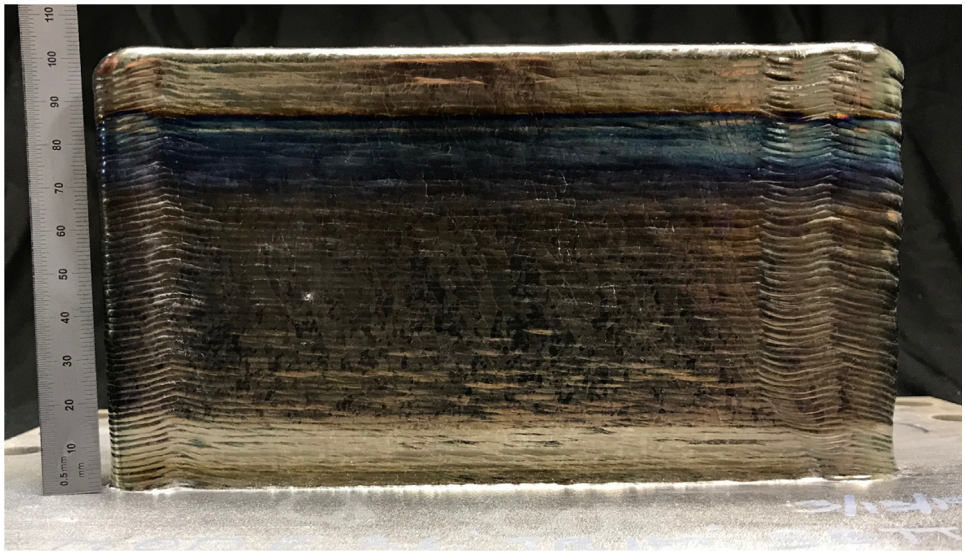

Fig. 7. Photograph of Single Bead Wall; Completed with Mode 3 of Operation.

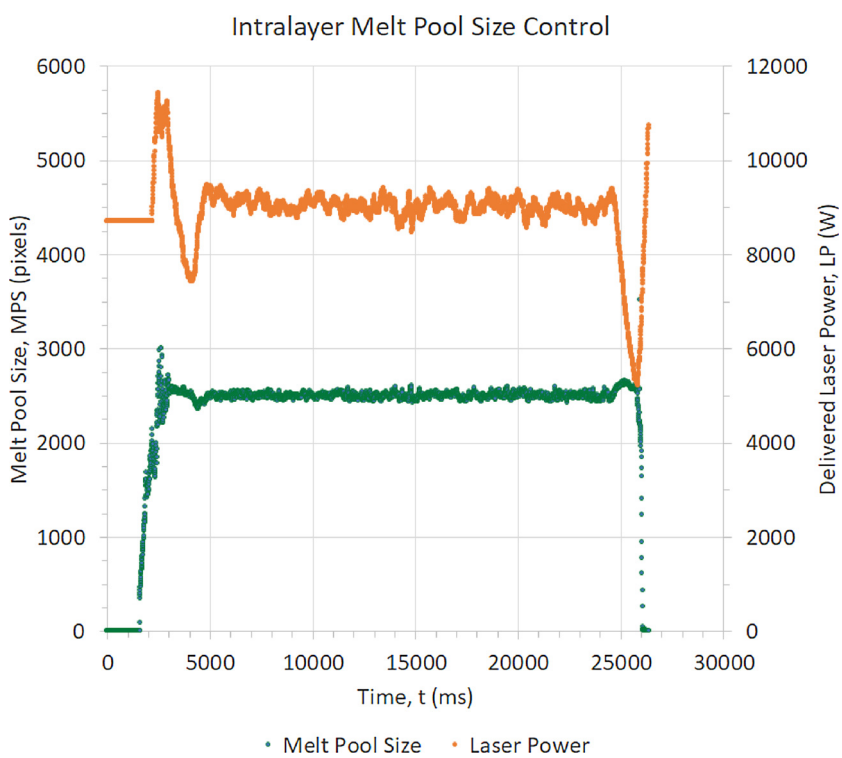

Fig. 8. Example of Intralayer Melt Pool Size Control; from Layer 1 of Single Bead Wall.

per layer basis; again, print speed and deposition rate are plotted as a single, normalized curve. The set-point for Mode 3 power was 9.01 kW, based on the average power of layer 1. Print speed increased from 8 mm/s to a peak of 10.77 mm/s and deposition rate proportionally increased from 2.4 kg/hr to a peak of 3.24 kg/hr, a 35 % increase. Total print time for the Mode 3 wall was 71.9 min, a more modest reduction in print time compared to the Mode 2 wall. Again, print speed saturators prevented speed reductions below nominal, which led to average laser power increases in the initial layers, as with Mode 1. Average laser power was controlled well, with a maximum average power error of 0.6 kW, which was experienced on layer 4, where power increases are actually desired in order to prevent wall width reductions; the greatest negative error was -0.56 kW, a 6.2 % error, on layer 56.

Wall geometries at the region of bead termination are compared via profiles at the mid-plane and 20 mm from the end of the walls, displayed in Fig. 13. It is important to note that the aspect ratio at which the wall profiles are displayed is somewhat deceiving, in that the data has been compressed in the Z-axis. At the mid-plane, the reduction in the wall width of the initial layers with Modes 0 and 2 is evident, whereas with Modes 1 and 3 wall width was maintained. The Mode 0 wall experienced the greatest overall width increase, as would be expected, and the Mode 1 and 3 wall widths tracked well together. The Mode 2 wall appeared to have the most consistent, vertical profile, while others trended toward the negative X direction. It is possible that factors such as build plate changeout between printing, the post-print scanning process, and profile alignment in data post-processing, were contributing to the perceived directionality of the profiles.

The bead termination profiles revealed the starkest contrasts in

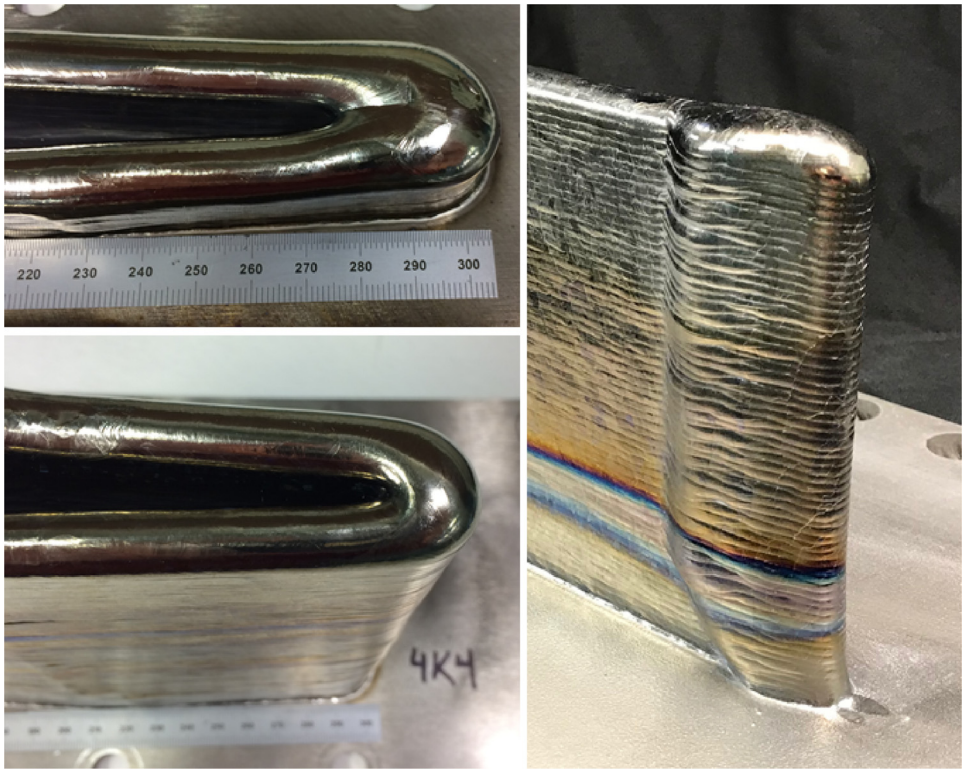

Fig. 9. Part Geometry Resulting from Various Control Modes: Contour with Mode 0 Control (top left), Contour with Mode 1 Control (bottom left), Region of Bead Termination on Single Bead Wall with Mode 2 Control.

control mode-dependent geometry. With Mode 0, the wall width increased most significantly, and there was a corresponding decrease in wall height, at a magnitude of approximately -4 mm in comparison to Modes 1–3. Mode 2 showed improvement, even without intralayer MPS control; again, this was reflected in the range of melt pool sizes documented in Fig. 11. Wall width was controlled best with Modes 1 and 3, whose profiles tracked well together and yielded consistent wall widths after some initial transient behavior in approximately the first 16 layers, which is likely related to the evolution of the bead termination routine parameters, particularly the reversal distance.

Finally, an interlayer energy density comparison among control modes is shown in Fig. 14. Energy density is a function of laser power, laser spot area, and print speed, and the formula is shown in Eq. 1.

$$Energy\ Density\ (ED) = \frac{Laser\ Power\ (LP)}{Spot\ Area\ (SA)\ \times\ Print\ Speed\ (PS)} \tag{1}$$

The laser spot diameter of the optics utilized in the study was 7.62 mm, and nominal energy density was 23.87 J/mm^3, as indicated in Fig. 14. Modes 1–3 reduced energy density in different ways during the printing of layered components. Energy density was reduced in Mode 1 through reductions in laser power. In Modes 2 and 3, energy density was reduced through increases in print speed, while laser power was maintained at nominal in Mode 2 and at a set-point through closed-loop control in Mode 3. Despite these differences, the overall reductions in energy density among the control modes were similar. In fact, the differences were perhaps not greater than the noise, with the exception that Mode 2 energy density may have trended slightly lower. Mode 2 energy density also did not increase above nominal in the initial layers

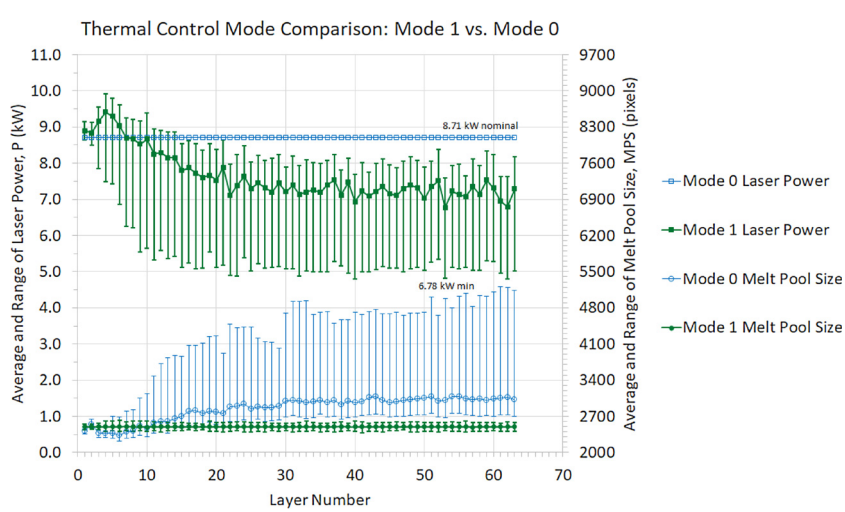

Fig. 10. Interlayer Behavior of Control Mode 0 and 1 Single Bead Walls.

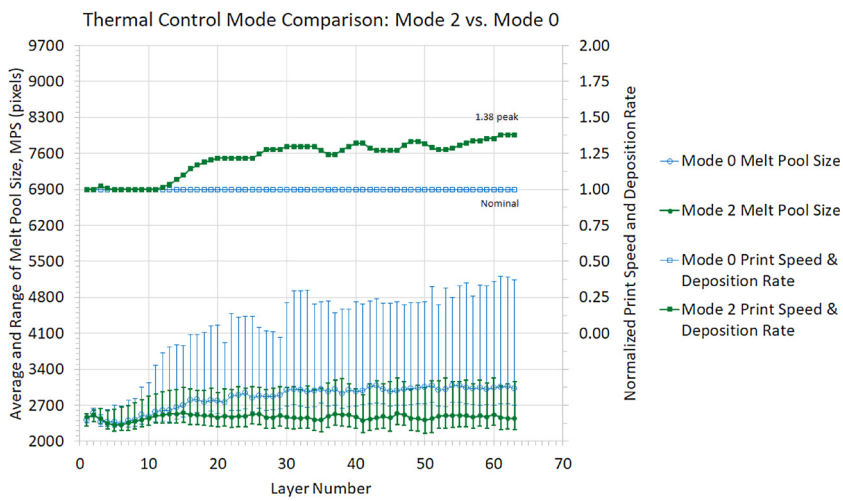

Fig. 11. Interlayer Behavior of Control Mode 0 and 2 Single Bead Walls.

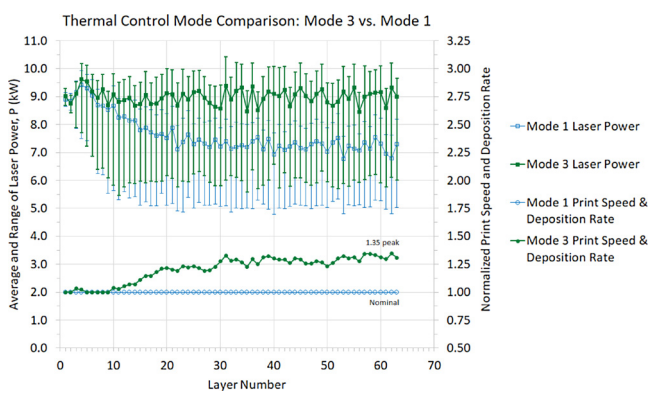

Fig. 12. Interlayer Behavior of Control Mode 1 and 3 Single Bead Walls.

due to the constraints on print speed, unlike Modes 1 and 3.

4. Discussion and conclusions

Melt pool size control yielded a fine, local control of bead geometry, particularly with Mode 1 control architecture. The controller was tuned and the through step changes in the MPS set-point were characterized by response times. Some slight differences in response times were

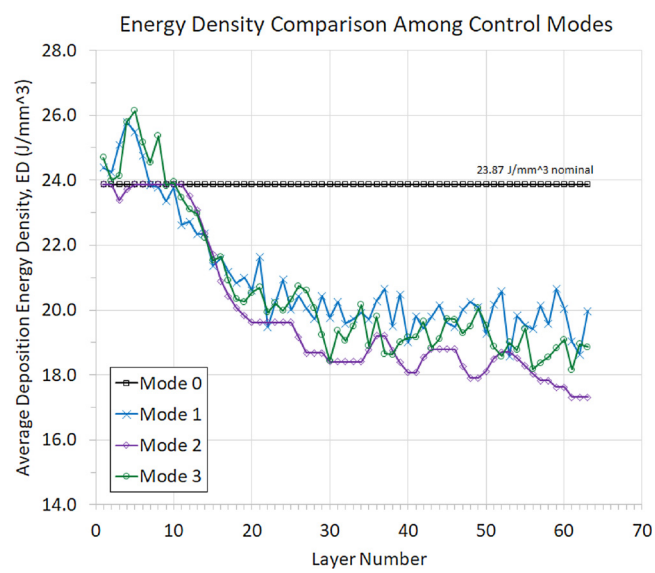

Fig. 14. Interlayer Energy Density Comparison Among Control Modes.

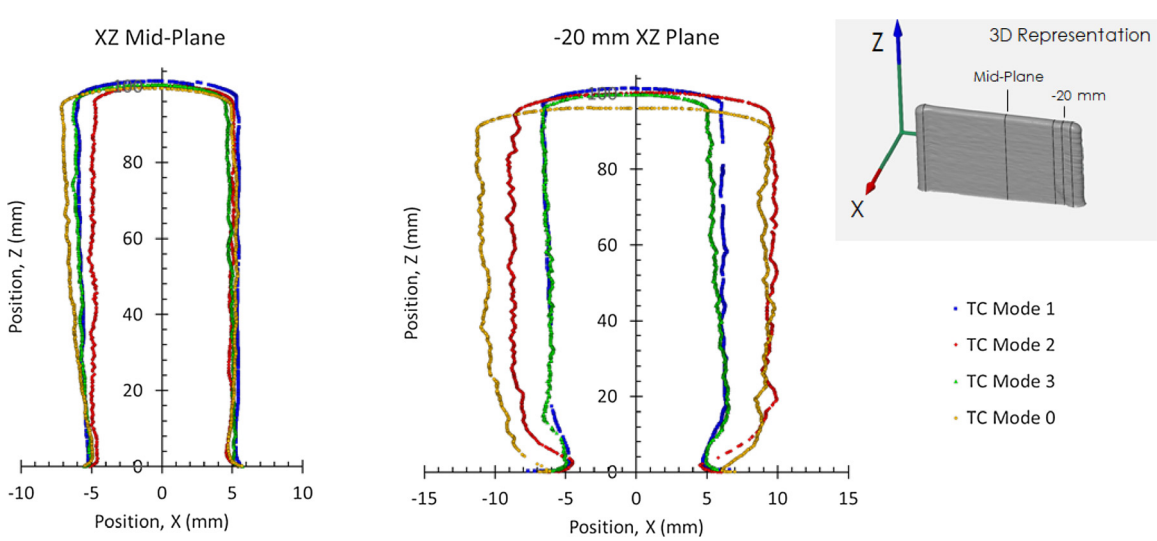

Fig. 13. Wall Geometry Profile Comparison Among Control Modes.

observed for cases of stepping down in MPS versus up. This can be attributed to the fact that, for decreases in MPS, the system is at the mercy of the thermal properties of the deposit and the natural frequency of the melt pool. In other words, localized, active cooling of the melt pool is not an option, at least not in the laser-wire DED process as it is currently implemented.

The thermal properties of the build were also evident in the print speed step change test, in which laser power was observed to have a slower, more gradual modulation in relation to the nearly instantaneous print speed changes. The print speed test highlighted another important aspect of the process: variations in bead profiles correlated with changes in process parameters under closed-loop MPS control. Bead height, rather than width, increased for the controlled case shown in Fig. 4, which could lead to interactions with other process control functions, such as the layer height control employed in the printing of walls in this study. The disturbance rejection test revealed a robust system capable of handling disturbances that were relatively large in magnitude.

The printing of a layered component with Mode 1 highlighted the fact that there is both fine, intralayer control and a coarse, interlayer effect associated with this control mode. Intralayer control was able to handle significant process transients, like that which occurred in the bead termination routine, and maintain the desired MPS and thus consistent bead geometry. The coarse interlayer effect was that of reducing average laser power on a per layer basis as heat accumulated in the component under construction. An approximate 23 % reduction in average laser power was observed through the progression of Mode 1 wall printing. As heat accumulates in the build, less laser power was required to achieve the desired MPS. This could be described as either a secondary heating effect or an insulating effect associated with the hot component under construction. While this reduction in laser power is acceptable and an inherent quality associated with Mode 1 control, it is somewhat undesirable from a production efficiency standpoint. What is more desirable is maintaining laser power and instead, increasing print speed and deposition rate, taking advantage of the accumulated heat in the build to maintain process stability.

Mode 2 was a control mode that isolated the effect of modulating print speed and deposition rate by controlling average MPS on a per-layer basis while maintaining a constant laser power. The printing of the Mode 2 wall demonstrated a reduction in total print time as well as improvements in global part geometry, compared to that of the Mode 0 wall, even as the lack of intralayer MPS control left something to be desired. Mode 3, however, combined the best attributes of Modes 1 and 2, combining intralayer MPS control with layerwise print speed and deposition rate modulations to control average laser power instead of average MPS, as with Mode 2. Total print time was again reduced with Mode 3, while the intralayer MPS control and resulting local bead and global part geometry properties were comparable to those of Mode 1. Achieving the desired global part geometry in particular is an important aspect to the high-levels goals of this work, in that printing near-net-shape parts to reduce the buy-to-fly ratio for aerospace pre-forms is economically impactful.

Finally, the examination of energy density underscored the fact that the controllers, regardless of mode, were reacting to the changing thermal conditions of the build. Because printing conditions were closely replicated during all the wall prints, similar reductions in energy density with respect to both the interlayer trend and overall magnitude were observed, regardless of control mode. This is important in that it eliminates energy density reduction as a distinguishing factor of the modes, giving the user freedom to focus on other aspects, such as geometry control, speed, and overall process efficiency, when choosing a control mode for part production. What remains understudied, however, and will be the focus of the continuing thread of this research, is the impact of control modes on within-layer and global thermal gradients, and on heating and cooling rates. These are important factors that drive material properties, residual stresses, and distortion. Characterizing the mode-dependent nature of these factors will be the focus of future work.

Funding and acknowledgements

This research was funded by the U.S. Department of Energy, Office of Energy Efficiency and Renewable Energy, Advanced Manufacturing Office in partnership with GKN Aerospace. The authors would like to acknowledge the contributions of the extended Oak Ridge National Laboratory and GKN Aerospace teams, particularly those of Brian Post, Alex Roschli, Michael Borish, and Abigail Barnes of ORNL and Aaron Thornton, John Potter, Ronnie Wilson, and Chris Allison of GKN Aerospace, along with Doug Bristow of the Missouri University of Science and Technology.

CRediT authorship contribution statement

B.T. Gibson: Conceptualization, Methodology, Software, Validation, Formal analysis, Investigation, Data curation, Writing - original draft, Visualization. **Y.K. Bandari:** Methodology, Investigation. **B.S. Richardson:** Investigation, Resources, Writing - review & editing, Supervision, Project administration. **W.C. Henry:** Conceptualization, Methodology. **E.J. Vetland:** Investigation, Data curation. **T.W. Sundermann:** Validation, Formal analysis, Data curation, Visualization. **L.J. Love:** Resources, Supervision, Project administration, Funding acquisition.

Declaration of Competing Interest

The authors declare that they have no known competing financial interests or personal relationships that could have appeared to influence the work reported in this paper.

References

[1] P. Aggarangsi, J.L. Beuth, M. Griffith, Melt pool size and stress control for laser-based deposition near a free edge, Proceedings of the Solid Freeform Fabrication Symposium (2003) 196–207.
[2] A. Vasinonta, J. Beuth, M. Griffith, Process maps for controlling residual stress and melt pool size in laser-based SFF processes, Proceedings of the Solid Freeform Fabrication Symposium (2000) 200–208.
[3] A. Vasinonta, J.L. Beuth, R. Ong, Melt pool size control in thin-walled and bulky parts via process maps, Proceedings of the Solid Freeform Fabrication Symposium (2001) 432–440.
[4] J. Beuth, N. Klingbeil, The role of process variables in laser-based direct metal solid freeform fabrication, JOM (September) (2001) 36–39.
[5] A. Birnbaum, P. Aggarangsi, J. Beuth, Process scaling and transient melt pool size control in laser-based additive manufacturing processes, Proceedings of the Solid Freeform Fabrication Symposium (2003) 328–339.
[6] P. Aggarangsi, J.L. Beuth, D.D. Gill, Transient changes in melt pool size in laser additive manufacturing process, Proceedings of the Solid Freeform Fabrication Symposium (2004) 163–174.
[7] F. Meriaudeau, F. Truchetet, C. Dumont, E. Renier, P. Bolland, Acquisition and image processing system able to optimize laser cladding process, Proceedings of ICSP (1996) 1628–1631.
[8] D. Hu, H. Mei, G. Tao, R. Kovacevic, Closed loop control of 3d laser cladding based on infrared sensing, Proceedings of the Solid Freeform Fabrication Symposium (2001) 129–137.
[9] W.H. Hofmeister, D.O. MacCallum, G.A. Knorovsky, Video monitoring and control of the LENS process, Proceedings of the 9th International Conference of Computer Technology in Welding, Detroit, MI, 1999, pp. 28–30 Sept.
[10] D. Hu, R. Kovacevic, Modelling and measuring the thermal behavior of the molten pool in closed-loop controlled laser-based additive manufacturing, Proc. Inst. Mech. Eng. Part B J. Eng. Manuf. 217 (2003) 441–452.
[11] J.M. Zalameda, E.R. Burke, R.A. Hafley, K.M.B. Taminger, C.S. Domack, A. Brewer, R.E. Martin, Thermal imaging for assessment of Electron-Beam Freeform Fabrication (EBF^3) additive manufacturing deposits, Proceedings of SPIE; Presented in Thermosense: Thermal Infrared Applications XXXV 8705 (2013).
[12] A. Heralic, A.K. Christiansson, K. Hurtig, M. Ottosson, B. Lennartson, Control design for automation of robotized laser metal-wire deposition, Proceedings of the 17th World Congress of The International Federation of Automatic Control, Seoul, Korea, 2008, pp. 6–11 July.
[13] B.T. Gibson, Y.K. Bandari, B.S. Richardson, A.C. Roschli, B.K. Post, M.C. Borish, A. Thornton, W.C. Henry, M. Lamsey, L.J. Love, Melt pool monitoring for control and data analytics in large-scale metal additive manufacturing, Proceedings of the

Solid Freeform Fabrication Symposium (2019) 1–18.
[14] M. Borish, B.K. Post, A. Roschli, P.C. Chesser, L.J. Love, K.T. Gaul, Defect identification and mitigation via visual inspection in large-scale additive manufacturing, JOM 71 (3) (2019) 893–899.
[15] D. Bristow, Melt pool measures and effective sensor bandwidth for direct energy deposition, International Solid Freeform Fabrication Symposium, Austin, TX, 2019, pp. 12–14. Aug.